The ∇B drift velocity of trapped particles in stellarators

V. V. Nemov and S. V. Kasilov
Institute of Plasma Physics, National Science Center, Kharkov Institute of Physics and Technology, Akademicheskaya str. 1, 61108 Kharkov, Ukraine

W. Kernbichler and G. O. Leitold
Institut für Theoretische Physik - Computational Physics, Technische Universität Graz, Petersgasse 16, A–8010 Graz, Austria

(Received 24 June 2005; accepted 11 October 2005; published online 28 November 2005)

In recent times, procedures for optimizing stellarator configurations have been strongly improved. New ideas and the development of pertinent codes allow an inclusion of various target functions into this optimization procedure. Here, new target functions which are related to collisionless α-particle confinement are introduced. They are based on specific averages of the bounce-averaged ∇B drift velocity of trapped particles across magnetic surfaces. This approach accompanies the frequently used computation of the effective ripple and it can be realized in a similar way using a field line tracing code. In addition, the poloidal motion of trapped particles is described in detail and results are discussed in the frame of an optimization study which aimed for a closure of contours of the second adiabatic invariant. © *2005 American Institute of Physics*. [DOI: 10.1063/1.2131848]

I. INTRODUCTION

The improvement of collisionless α-particle confinement in stellarators is one of the key issues in stellarator optimization problems (see, e.g., Refs. 1 and 2). In the long-mean-free-path regime characteristic for thermonuclear plasma applications, the particle confinement in stellarators is mainly determined by confinement of trapped particle orbits. Due to the lack of axisymmetry in stellarators these orbits can undergo large excursions from magnetic surfaces. This effect significantly depends on the specific magnetic-field geometry of the stellarator.

The most consequent approach for the investigation of collisionless particle confinement is realized in codes which perform a direct computation of particle losses. In these codes the guiding center drift equation is used to follow trapped particle orbits until such particles are lost (see, e.g., Refs. 3 and 4). Such a kind of code requires long computing times because of the fact that one has to follow a huge sample of particles with starting points evenly distributed in space as well as in pitch angles.

Therefore, for an optimization of the collisionless α-particle confinement in stellarators it would be desirable to have simple criteria, finally, resulting in much faster numerical evaluation times. Such criteria can be connected with the minimization of quantities such as the geodesic curvature of magnetic-field lines, the residuals in the magnetic spectrum of quasisymmetric systems (nonquasisymmetric components), the effective ripple in the $1/\nu$ regime, the WATER parameter (minimization of ripple-well areas along a field line), etc. (see Refs. 5 and 6). Based on the experience with those existing criteria, the present work proposes a set of new criteria which are based on the computation of the bounce-averaged ∇B drift velocity of trapped particles across magnetic surfaces. For this purpose, two new target functions which are further denoted as Γ_v and Γ_w are introduced. Absolute confinement of trapped particles is guaranteed when these target functions are zero.

In Ref. 7, this drift velocity v_{an} has been studied in terms of a variation of the second adiabatic invariant $J_{\parallel}=\oint v_{\parallel} ds$ on a magnetic surface. The quantity v_{an} can be presented as a two-dimensional function of the position of the local minimum of B, where the charged particle is trapped and of the value of the pitch angle at this local minimum. Here, B is the modulus of the magnetic-field strength. Following from this, the quantity Γ_v is obtained as a result of a mean-square average of v_{an} over the magnetic surface and over the phase volume for trapped particles using the distribution function of trapped particles as a weight function. In addition, the quantity Γ_w represents the integral effect of the square of the ∇B drift velocity for all trapped particles within a magnetic surface.

A sufficiently large velocity of the poloidal motion of trapped particles promotes the formation of poloidally closed contours of $J_{\parallel}$. These closed contours are of high importance for trapped particle confinement. Therefore, together with the radial ∇B drift also the poloidal motion of trapped particles is discussed in the present paper.

The present paper also shows results for a variety of stellarator magnetic configurations for which the neoclassical confinement properties have been studied earlier using different methods. Numerical results for Γ_v and Γ_w are computed using a field line tracing code. The results are compared to effective ripple computations performed according to the method given in Ref. 8. This is of interest because the so-called effective ripple characterizes the $1/\nu$ neoclassical transport in stellarators. It is frequently used as an optimization target but its minimization does not necessarily enforce optimized α-particle confinement. Of course, also the $1/\nu$ neoclassical transport in stellarators is caused partly by the bounce-averaged ∇B drift of trapped particles across the

magnetic surfaces, but, in addition, also collision processes play an important role there and are obviously responsible for the differences.

II. DERIVATION OF Γ_w AND Γ_v

For an arbitrary stellarator magnetic field, the bounce-averaged drift velocity v_{an} can be presented as[7,8]

$$v_{an} = \frac{\delta\psi}{\tau_b \langle |\nabla\psi| \rangle}, \tag{1}$$

with ψ being the magnetic surface label, τ_b being the bounce time, and $\delta\psi$ being an increment in ψ during τ_b. Averaging of $|\nabla\psi|$ is performed by the rule

$$\langle A \rangle = \lim_{L\to\infty} \left(\int_0^L \frac{ds}{B} \right)^{-1} \int_0^L ds \frac{A}{B}, \tag{2}$$

with s being the length along the magnetic-field line. Every trapped particle is trapped within a certain segment of the magnetic-field line limited by the turning points $s_j^{\min}$ and $s_j^{\max}$, where j numbers the segments along the magnetic-field line. With this definition one can express the bounce time $\tau_{b,j}$ and the displacement $\delta\psi_j$ as

$$\tau_{b,j} = \oint_{(j)} \frac{ds}{v_\parallel} = 2 \int_{s_j^{\min}}^{s_j^{\max}} \frac{ds}{|v_\parallel|}, \tag{3}$$

$$\delta\psi_j = \oint_{(j)} \frac{ds}{v_\parallel} \mathbf{v}\cdot\nabla\psi = 2 \int_{s_j^{\min}}^{s_j^{\max}} \frac{ds}{|v_\parallel|} \mathbf{v}\cdot\nabla\psi, \tag{4}$$

where $v_\parallel(\mathbf{r}, w, J_\perp) = \sigma\sqrt{v^2 - J_\perp B}$, $v^2 = 2(w - e\phi)/m$, $J_\perp = v_\perp^2/B$, and $\sigma = \pm 1$. Using the explicit expression for the guiding center drift velocity and the fact that for an equilibrium magnetic field $(\nabla\times\mathbf{B})\cdot\nabla\psi = 0$ one obtains

$$\frac{\mathbf{v}\cdot\nabla\psi}{|v_\parallel|} = \left(\frac{v^2}{|v_\parallel|} + |v_\parallel| \right) \frac{|\nabla\psi| k_G}{2\omega_c} = -\frac{\partial}{\partial J_\perp} \left(v^2 |v_\parallel| + \frac{1}{3} |v_\parallel|^3 \right) \frac{|\nabla\psi| k_G}{B\omega_c}, \tag{5}$$

where $\omega_c = eB/(mc)$, $\mathbf{h}$ is the unit vector $\mathbf{h} = \mathbf{B}/B$, and k_G is the geodesic curvature of the magnetic-field line,

$$|\nabla\psi| k_G = [\mathbf{h}\times(\mathbf{h}\cdot\nabla)\mathbf{h}]\cdot\nabla\psi = \frac{1}{B^2}(\mathbf{B}\times\nabla B)\cdot\nabla\psi. \tag{6}$$

With $1/v_\parallel$ in the following form:

$$\frac{1}{v_\parallel} = -\frac{2}{B}\frac{\partial v_\parallel}{\partial J_\perp}, \tag{7}$$

and substituting (7) and (5) into (3) and (4) one obtains

$$\delta\psi_j = -\frac{1}{3}\frac{\partial H_j}{\partial J_\perp}, \tag{8}$$

$$H_j = 2 \int_{s_j^{\min}}^{s_j^{\max}} \frac{ds}{B} |v_\parallel| (3v^2 + v_\parallel^2) \frac{|\nabla\psi| k_G}{\omega_c}, \tag{9}$$

and

$$\tau_{b,j} = -2\frac{\partial I_j}{\partial J_\perp}, \tag{10}$$

$$I_j = 2 \int_{s_j^{\min}}^{s_j^{\max}} \frac{ds}{B} |v_\parallel|. \tag{11}$$

Introducing the new variable b' connected with $J_\perp$ as $b' = v^2/(J_\perp B_0)$, where B_0 is some reference magnetic field, one finally obtains

$$\delta\psi_j = \frac{2B_0 v b'^2}{\omega_{c0}} \frac{\partial g_j}{\partial b'}, \tag{12}$$

$$\tau_{b,j} = \frac{4B_0 b'^2}{v} \frac{\partial \hat{I}_j}{\partial b'}, \tag{13}$$

with $\omega_{c0} = eB_0/(mc)$ and

$$g_j = \frac{1}{3} \int_{s_j^{\min}}^{s_j^{\max}} \frac{ds}{B} \sqrt{1 - \frac{B}{B_0 b'}} \left(4\frac{B_0}{B} - \frac{1}{b'} \right) |\nabla\psi| k_G, \tag{14}$$

$$\hat{I}_j = \int_{s_j^{\min}}^{s_j^{\max}} \frac{ds}{B} \sqrt{1 - \frac{B}{B_0 b'}}. \tag{15}$$

From the last expressions and (1) one obtains

$$v_{an} = \frac{\delta\psi}{\tau_b \langle |\nabla\psi| \rangle} = \frac{v^2}{2\omega_{c0} \langle |\nabla\psi| \rangle} \frac{\partial g_j/\partial b'}{\partial \hat{I}_j/\partial b'}. \tag{16}$$

For a certain trapped particle v_{an} (16) is a function of its energy w and its perpendicular adiabatic invariant $J_\perp$. To determine the proposed integral effect of the ∇B drift one has to integrate v_{an}^2 over the phase-space volume for the distribution of trapped particles, f, and perform an average over the magnetic surface according to

$$F_n^* = \frac{1}{S} \oint_{(S)} dS \int v_{an}^2 f d\Gamma_{w,J_\perp}, \tag{17}$$

where $f = f(w,\psi)$ and $d\Gamma_{w,J_\perp}$ is the phase-space volume element:

$$d\Gamma_{w,J_\perp} = \sum_{\sigma=\pm 1} \frac{\pi B}{m|v_\parallel|} dJ_\perp dw = \frac{2\pi B}{m|v_\parallel|} dJ_\perp dw. \tag{18}$$

From (17) and (18) follows

$$F_n^* = \frac{1}{S} \oint dS \int_{e\Phi}^{\infty} dw \int_{J_{\perp\min}}^{J_{\perp\max}} dJ_\perp \frac{2\pi B}{m|v_\parallel|} f v_{an}^2, \tag{19}$$

with $J_{\perp\min} = v^2/B_{\max}^{abs}$ and $J_{\perp\max} = v^2/B$. After substituting (16) into (19) the integration over the magnetic surface area is transformed to an integration over the volume between neighboring magnetic surfaces.[8] Using the equivalence between averages over this volume and averages along magnetic-field lines, one obtains the following expression:

$$F_n^* = \frac{\sqrt{2}}{m} \frac{1}{R_0^2 \omega_{c0}^2} \Gamma_w \int_{e\Phi}^{\infty} dw v^5 f, \tag{20}$$

with Γ_w being defined as

$$\Gamma_w = \frac{\pi R_0^2}{\sqrt{2}} \lim_{L_s\to\infty}\left(\int_0^{L_s}\frac{ds}{B}\right)^{-1}\frac{1}{\langle|\nabla\psi|\rangle^2} \times \int_{B_{\min}^{\mathrm{abs}}/B_0}^{B_{\max}^{\mathrm{abs}}/B_0} db' \sum_{j=1}^{j_{\max}}\left(\frac{\partial g_j}{\partial b'}\right)^2\left(\frac{\partial \hat{I}_j}{\partial b'}\right)^{-1}. \quad (21)$$

Here, R_0 is the major radius of the torus, B_0 is the reference magnetic field, and $B_{\min}^{\mathrm{abs}}$ and $B_{\max}^{\mathrm{abs}}$ are the absolute minimum and maximum of B within the sufficiently large interval $(0,L_s)$, respectively. The index j is numbering the field line intervals $(s_j^{\min}, s_j^{\max})$, where $b'-B/B_0 \geqslant 0$ for a given $J_\perp$ and w. The representation in (21) has the advantage that it can be computed efficiently in a field line tracing code.

In an analysis of collisionless α-particle losses (see, e.g., Ref. 4) an approach with the Larmor radius being constant is often used. To be close to such an approach, here a monoenergetic distribution function

$$f = n\frac{m^{3/2}}{4\sqrt{2}\pi\sqrt{E-e\Phi}}\delta(w-E) \quad (22)$$

is used in (20). A substitution of (22) into (20) results in the final form,

$$F_n^* = \frac{\sqrt{2}}{4\pi}\Gamma_w\frac{v^2\rho_L^2}{R_0^2}n, \quad (23)$$

with $\rho_L = v/\omega_{c0}$ being the characteristic Larmor radius and $v^2 = 2(E-e\Phi)/m$.

The phase volume of the trapped particles averaged over a magnetic surface with the weight f is determined by the following expression:

$$V^* = \frac{1}{S}\oint dS\sum_{\sigma=\pm1}\int_{e\Phi}^{\infty}dw\int_{J_{\perp\min}}^{J_{\perp\max}}dJ_\perp\frac{\pi B}{m|v_\parallel|}f = \frac{4\pi}{mS}\oint dS\sqrt{1-\frac{B}{B_{\max}^{\mathrm{abs}}}}\int_{e\Phi}^{\infty}dwvf. \quad (24)$$

Substituting (22) into (24) one finally obtains

$$V^* = n\frac{2\sqrt{2}}{\pi}\Gamma_s, \quad (25)$$

with

$$\Gamma_s = \frac{\pi}{2\sqrt{2}}\frac{1}{\langle|\nabla\psi|\rangle}\left\langle|\nabla\psi|\sqrt{1-\frac{B}{B_{\max}^{\mathrm{abs}}}}\right\rangle. \quad (26)$$

Starting from (21) and (26), one can conveniently use the definitions

$$\hat{v}_{\mathrm{an}}^2 = \frac{F_n^*}{V^*} \quad (27)$$

and

$$\Gamma_v = \sqrt{\frac{\Gamma_w}{\Gamma_s}} \quad (28)$$

to formulate the mean-square average of the bounce-averaged ∇B drift velocity of trapped particles across a magnetic surface as

$$\hat{v}_{\mathrm{an}} = \frac{1}{2\sqrt{2}}\Gamma_v\frac{\rho_L}{R_0}v. \quad (29)$$

It should be noted here that if one uses the Maxwellian distribution instead of the monoenergetic distribution (22), the following expressions for F_n^* and $\hat{v}_{\mathrm{an}}$ are obtained:

$$F_n^* = \frac{15\sqrt{2}}{16\pi}\Gamma_w\frac{v_T^2\rho_{\mathrm{LT}}^2}{R_0^2}n, \quad (30)$$

and

$$\hat{v}_{\mathrm{an}} = \sqrt{\frac{15}{32}}\Gamma_v\frac{\rho_{LT}}{R_0}v_T, \quad (31)$$

respectively, where $\rho_{\mathrm{LT}} = v_T/\omega_{c0}$ is the mean Larmor radius and $v_T = \sqrt{2T/m}$ is the thermal velocity.

The magnetic field of a conventional stellarator with circular cross sections of magnetic surfaces and a sufficiently large aspect ratio can be presented as

$$B \approx B_0[1+\epsilon_h\cos(m\theta - n\varphi)]. \quad (32)$$

For such a model, the calculation of the factors Γ_w, Γ_v, and Γ_s results in

$$\Gamma_w^{(\mathrm{conv})} = \sqrt{\epsilon_h}, \quad (33)$$

$$\Gamma_s^{(\mathrm{conv})} = \sqrt{\epsilon_h}, \quad (34)$$

$$\Gamma_v^{(\mathrm{conv})} = 1, \quad (35)$$

respectively. Note that the numerical factors in (20) and (25) are chosen in a way to ensure this simple representation.

In principle, for a numerical evaluation of Γ_w (21) as well as v_{an} (16) along the magnetic-field line two approaches are possible. In the first approach calculations of g_j and $\hat{I}_j$ are performed using formulas (14) and (15) followed by a numerical differentiation with respect to b' to obtain $\partial g_j/\partial b'$ and $\partial\hat{I}_j/\partial b'$. Contrary, in the second approach the subintegrands in formulas (14) and (15) are differentiated analytically with respect to b' and then used directly as new subintegrands. It should be noted that there is no general answer to which of the two approaches is to be favored. Depending on the magnetic configuration there seems to be advantages of one over the other.

An important role in the numerical computation of the Γ parameters belongs to the computation of the quantity $\nabla\psi$. In case of a real-space representation of the magnetic field, formulas for the Γ parameters should be supplemented with the magnetic-field line equations as well as with equations for the vector $\mathbf{P}\equiv\nabla\psi$ (see, e.g., Refs. 8 and 9),

$$\frac{dP_i}{ds} = -\frac{1}{B}\frac{\partial B^j}{\partial\xi^i}P_j, \quad (36)$$

where B^j are the contravariant components of $\mathbf{B}$ in real-space coordinates ξ^i and $P_j = \partial\psi/\partial\xi^j$ are the covariant components of $\mathbf{P}$.

For computations in Boozer magnetic coordinates[10] the quantity $|\nabla\psi|k_G$ is calculated using the Boozer spectrum of B as well as Boozer spectra of cylindrical coordinates of the magnetic surfaces.[8,11]

III. POLOIDAL MOTION OF THE TRAPPED PARTICLES

When describing the motion of the trapped particles in terms of the second adiabatic invariant $J_\parallel = \oint v_\parallel ds$, the variation of $J_\parallel$ on a magnetic surface ψ=const is directly related to the trapped particle motion across this surface. If this variation is nonzero, then a sufficiently large derivative of $J_\parallel$ with respect to ψ, $\partial J_\parallel/\partial\psi$, is necessary to obtain poloidally closed contours of $J_\parallel$. Within a Clebsch representation of $\mathbf{B}$, $\mathbf{B}=\nabla\psi\times\nabla\theta_0$, the poloidal motion of trapped particles is characterized by the increment of θ_0, $\Delta\theta_0$, during one bounce period. With this, $\Delta\theta_0$ is proportional to the quantity $\partial J_\parallel/\partial\psi$ where $J_\parallel = J_\parallel(\psi,\theta_0)$.

This indicated representation of $\mathbf{B}$ is connected with the coordinates ψ, θ_0, and ζ, where ζ is counted along the magnetic-field line. A peculiarity of these coordinates is that in toroidal geometry they are not periodic. Usually, for a study of different questions in stellarator geometry in magnetic coordinates, periodic Boozer coordinates[10] (ψ,θ,φ) are used, corresponding to $\zeta=\varphi$ and $\theta_0=\theta-\iota\varphi$, with $2\pi\psi$ being the toroidal magnetic flux and $\iota=\iota(\psi)$ being the rotational transform in units of 2π.

In this case it is convenient to describe the poloidal motion of trapped particles with the increment of θ during one bounce period, $\Delta\theta$, and not with $\Delta\theta_0$. From the relation between θ and θ_0 one can derive

$$\frac{d\theta}{dt} = \frac{d\theta_0}{dt} + \iota\frac{d\varphi}{dt} + \varphi\iota'\frac{d\psi}{dt}, \tag{37}$$

where the prime denotes the derivative with respect to ψ. To find the derivatives of ψ, θ_0, and φ one can use the equations for particle motion (3.41) of Ref. 12 which in ψ, θ_0, φ notation are given as

$$\frac{d\psi}{dt} = \frac{cv_\parallel}{eB\sqrt{g}}\left[\frac{\partial}{\partial\theta_0}(mv_\parallel h_\varphi) - \frac{\partial}{\partial\varphi}(mv_\parallel h_{\theta_0})\right], \tag{38}$$

$$\frac{d\theta_0}{dt} = \frac{cv_\parallel}{eB\sqrt{g}}\left[\frac{\partial}{\partial\varphi}(mv_\parallel h_\psi) - \frac{\partial}{\partial\psi}(mv_\parallel h_\varphi)\right], \tag{39}$$

$$\frac{d\varphi}{dt} \approx v_\parallel h^\varphi, \tag{40}$$

where $\sqrt{g}=1/(\nabla\psi\times\nabla\theta_0\cdot\nabla\varphi)$, $h^\psi=h^{\theta_0}=0$, and $h^\varphi=1/(B\sqrt{g})$. Substituting (38)–(40) into (37) and integrating with respect to t one finds

$$\Delta\theta = \iota\Delta\varphi - \frac{c}{e}\int\left[\frac{\partial}{\partial\psi}(mv_\parallel h_\varphi) - \varphi\iota'\frac{\partial}{\partial\theta_0}(mv_\parallel h_\varphi)\right]d\varphi + \frac{c}{e}\int\frac{\partial}{\partial\varphi}(mv_\parallel h_\psi)d\varphi - \iota'\frac{c}{e}\int\varphi\frac{\partial}{\partial\varphi}(mv_\parallel h_{\theta_0})d\varphi. \tag{41}$$

Taking the integrals in (41) over an interval of φ corresponding to one bounce period and noting that $\Delta\varphi=0$ one obtains

$$\Delta\hat{\theta} = -\frac{c}{e}\oint\left[\frac{\partial}{\partial\psi}(mv_\parallel h_\varphi) - \varphi\iota'\frac{\partial}{\partial\theta_0}(mv_\parallel h_\varphi)\right]d\varphi + \iota'\frac{c}{e}\oint mv_\parallel h_{\theta_0}d\varphi. \tag{42}$$

For a Boozer representation of $\mathbf{B}$, $\sqrt{g}=(F+\iota I)/B^2$, $h_{\theta_0}=I/B$, and $h_\varphi=(F+\iota I)/B$, with $cF(\psi)/2$ and $cI(\psi)/2$ being the poloidal (external with respect to the magnetic surface) and toroidal electric currents, respectively. With this it follows from (42),

$$\Delta\hat{\theta} = \Delta\hat{\theta}_{\nabla B} + \Delta\hat{\theta}_E - \frac{mc}{e}\frac{(F'+\iota I')}{(F+\iota I)}J_\parallel, \tag{43}$$

where

$$\Delta\hat{\theta}_{\nabla B} = \frac{mc}{e}\oint\frac{\partial B}{\partial\psi}\frac{(v_\parallel^2 + (1/2)J_\perp B)}{v_\parallel B}\frac{(F+\iota I)}{B}d\varphi, \tag{44}$$

$$\Delta\hat{\theta}_E = c\Phi'\oint\frac{1}{v_\parallel}\frac{(F+\iota I)}{B}d\varphi = c\Phi'\tau_b, \tag{45}$$

$$J_\parallel = \oint v_\parallel\frac{(F+\iota I)}{B}d\varphi = 2\int_{s_j^{\min}}^{s_j^{\max}}|v_\parallel|ds. \tag{46}$$

The equality $(F+\iota I)d\varphi = Bds$ is used in (45) and (46). Note also that in (44) B is used as $B=B(\psi,\theta,\varphi)$ in contrast to (42) where $B=B(\psi,\theta_0,\varphi)$ and

$$\left(\frac{\partial}{\partial\psi} - \varphi\iota'\frac{\partial}{\partial\theta_0}\right)B(\psi,\theta_0,\varphi) = \frac{\partial}{\partial\psi}B(\psi,\theta,\varphi). \tag{47}$$

According to the equalities

$$v_\parallel = -\frac{\partial}{\partial J_\perp}\left(\frac{2v_\parallel^3}{3B}\right), \tag{48}$$

$$\frac{v_\parallel^2 + (1/2)J_\perp B}{v_\parallel} = -\frac{\partial}{\partial J_\perp}\left[\frac{1}{B}v_\parallel\left(v^2 + \frac{1}{3}v_\parallel^2\right)\right], \tag{49}$$

expressions (44) and (46) can be presented as

$$\Delta\hat{\theta}_{\nabla B} = -\frac{mc}{e}\frac{\partial G_j}{\partial J_\perp}, \tag{50}$$

$$J_\parallel = \frac{\partial K_j}{\partial J_\perp}, \tag{51}$$

with

$$G_j = 2\int_{s_j^{\min}}^{s_j^{\max}} \frac{1}{B^2}\frac{\partial B}{\partial \psi}|v_\parallel|\left(v^2+\frac{1}{3}v_\parallel^2\right)ds, \tag{52}$$

$$K_j = -\frac{4}{3}\int_{s_j^{\min}}^{s_j^{\max}} |v_\parallel|^3\frac{ds}{B}. \tag{53}$$

Now introducing the definition

$$\frac{d\theta}{dt} = \frac{\Delta\hat{\theta}}{\tau_b}, \tag{54}$$

and using again the pitch-angle variable b' and Eq. (13) for τ_b one finally obtains

$$\frac{d\theta}{dt} = \frac{v^2 B_0}{2\omega_{c0}}\left[\frac{\partial\hat{G}_j/\partial b'}{\partial\hat{I}_j/\partial b'} - \frac{2}{3}\frac{(F'+\iota I')}{(F+\iota I)}\frac{\partial\hat{K}_j/\partial b'}{\partial\hat{I}_j/\partial b'} + \frac{2e}{mv^2}\Phi'\right], \tag{55}$$

where

$$\hat{G}_j = \frac{1}{3}\int_{s_j^{\min}}^{s_j^{\max}}\frac{ds}{B}\sqrt{1-\frac{B}{B_0 b'}}\left(4\frac{B_0}{B}-\frac{1}{b'}\right)\frac{1}{B}\frac{\partial B}{\partial\psi}, \tag{56}$$

$$\hat{K}_j = \int_{s_j^{\min}}^{s_j^{\max}}\frac{ds}{B}\left(1-\frac{B}{B_0 b'}\right)^{3/2}. \tag{57}$$

Some results for Eq. (55) are given in Sec. VI.

IV. COMPUTATIONS OF Γ_w AND Γ_v

In the present section, the proposed technique for computing the optimization targets Γ_w and Γ_v is illustrated for a number of stellarator configurations. For this purpose, a field line tracing code was developed being able to operate with configurations given in real-space coordinates as well as in Boozer magnetic coordinates:[10] (i) a test configuration specified with the help of a single toroidal harmonic function; (ii) the idealized Wendelstein 7-X (W7-X) standard high-mirror configuration[13] as well as the quasihelically symmetric (QHS) stellarator;[14] and (iii) two quasi-isodynamical stellarator configurations with poloidally closed contours of B on magnetic surfaces.[15] In general, the configurations are characterized by the big torus radius R and by the number of field periods along the torus, n_p. The computational results are presented as functions of r/a, with r being the mean radius of a given magnetic surface and a being the mean radius of the outermost magnetic surface.

A. $l=3$ stellarator-type magnetic field

In order to confirm the validity of the approach and the correctness of the code, two simple "classical" configurations are chosen where the magnetic field in real-space coordinates is expressed with the help of a single toroidal harmonic function, the associated Legendre function with the following parameters: $l=3$ and $a=10$ cm for both configurations; (i) $n_p=9$, $R=10^2$ cm; and (ii) $n_p=900$, $R=10^4$ cm. The aspect ratio of the second configuration is 100 times larger but the number of field periods was chosen in such a way that the length of one magnetic-field period is the same. In addition, the amplitudes of the harmonics were adjusted to give roughly the same rotational transform per field period and thus resulting in the same ϵ_h.

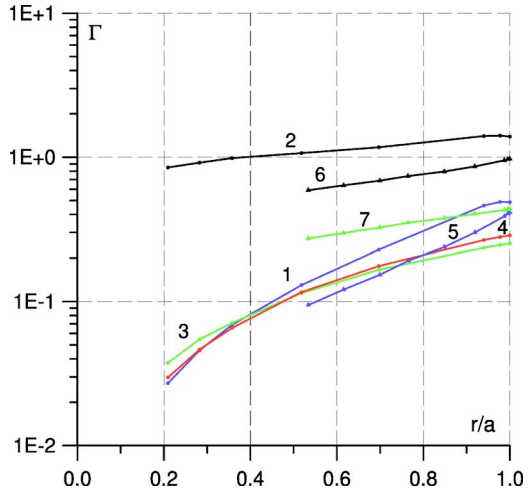

FIG. 1. Factors Γ_w, Γ_v, and Γ_s for $l=3$ magnetic field with $R_T=10^2$ cm and $R_T=10^4$ cm: 1: Γ_w for $R_T=10^4$ cm; 2: Γ_v for $R_T=10^4$ cm; 3: Γ_s for $R_T=10^4$ cm; 4: $\sqrt{\epsilon_h}$ for $R_T=10^4$ cm; 5: Γ_w for $R_T=10^2$ cm; 6: Γ_v for $R_T=10^2$ cm; 7: Γ_s for $R_T=10^2$ cm.

Computational results for these $l=3$ configurations are presented in Fig. 1. As expected in the inner range ($0.3 \leqslant r/a \leqslant 0.5$), the factors Γ_w and Γ_s for the second set of parameters are close to each other and very close to $\sqrt{\epsilon_h}$ (curve 4) which was found from the modulation of B along magnetic-field lines. As a result, Γ_v turns out to be very close to unity and one gets almost the results for a conventional stellarator with a big aspect ratio (33)–(35). For the outer region ($r/a>0.5$) results slightly differ from those of the conventional stellarator because the triangular shape of the magnetic surfaces of an $l=3$ configuration manifests itself more pronounced in this outer region. Results for the first case show a similar behavior but with a slightly larger deviation from the theoretical predictions (33)–(35). This is to be expected because the much smaller aspect ratio is also limiting the validity of the predictions.

B. Wendelstein 7-X and QHS

In Fig. 2, results for two neoclassically optimized stellarator configurations are shown, namely, for the idealized W7-X configuration[13] (standard, high-mirror configuration, $n_p=5$) and for the QHS stellarator configuration[14] ($n_p=6$). The magnetic-fields for both configurations are presented in real-space coordinates and expressed through a series of a big but finite number of toroidal harmonic functions (480) containing the associated Legendre functions. The decomposition coefficients for these series are computed using the information on boundary surfaces of the equilibria in magnetic coordinates presented in Refs. 13 and 14. Some features of neoclassical confinement in these configurations have already been studied in Refs. 7, 8, and 16.

For these configurations, Γ_w and Γ_v are much smaller than those for the conventional stellarator. Compared to the result for the conventional stellarator, the parameter Γ_v is

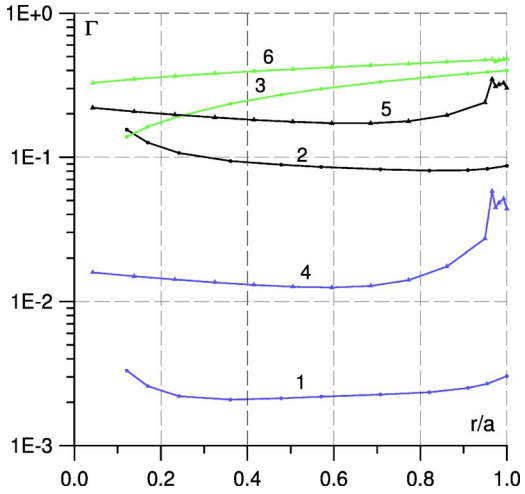

FIG. 2. Factors Γ_w, Γ_v, and Γ_s for the magnetic configurations of W7-X and QHS: 1: Γ_w for QHS; 2: Γ_v for QHS; 3: Γ_s for QHS; 4: Γ_w for W7-X; 5: Γ_v for W7-X; 6: Γ_s for W7-X.

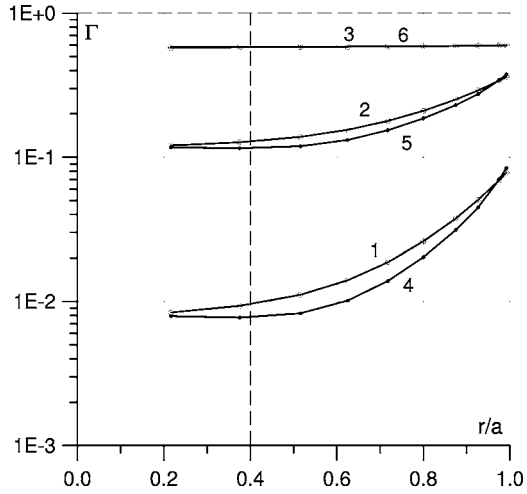

FIG. 3. Factors Γ_w, Γ_v, and Γ_s for the quasi-isodynamical (QI) magnetic configurations: 1: Γ_w for the first configuration; 2: Γ_v for the first configuration; 3: Γ_s for the first configuration; 4: Γ_w for the second configuration; 5: Γ_v for the second configuration; 6: Γ_s for the second configuration.

approximately 5 times smaller for W7-X and even 10 times smaller for QHS. This is in good agreement with the corresponding evaluation of v_{an} presented in Ref. 7. One should note that the irregularities in Γ_w and Γ_v for W7-X near the boundary (curves 4 and 5) are caused by an island structure around the surface with the rotational transform $\iota=1$.

The last results demonstrate the possibility of the proposed technique to perform the calculations in magnetic islands if the magnetic field is given in real-space coordinates. For this case, there is no difference in studies for nonisland and island magnetic surfaces. In contrast, when the magnetic field is given in magnetic coordinates the analogous calculations are impossible for magnetic islands since the data sets obtained in magnetic coordinates from three-dimensional magnetohydrodynamic equilibrium codes (see, e.g., Ref. 1) do not contain information about magnetic islands.

C. Quasi-isodynamical configurations

The quasi-isodynamical (QI) configurations[15] with $n_p=6$ are the result of an optimization of such configurations with respect to collisionless particle confinement (first QI configuration) and subsequent optimization towards poloidal closure of the $J_\parallel$ contours (second QI configuration[15]). So, the first configuration is the result before the final optimization step. Results for Γ_w and Γ_v in Fig. 3 confirm this final optimization step with smaller values for the second QI configuration compared to the first QI configuration in a wide inner region of the configuration. Only in a very small region at the edge, this tendency is reversed. The Γ_s values are practically the same for both configurations.

As expected, the second configuration is preferable compared to the first one. To assess a measure for the achieved optimization, the results for Γ_w and Γ_v of this second configuration are plotted together with the results for W7-X and QHS in Fig. 4. Here one sees that the very good results for QHS cannot be reached and that the results for the final optimization step of the QI configuration and for W7-X are rather close. There is a small advantage of the QI configuration in the inner region (roughly a factor of 2) which turns at $r/a=0.7$ into a similar advantage of W7-X in the outer region of the device.

V. COMPARISON WITH EFFECTIVE RIPPLE COMPUTATIONS

The bounce-averaged ∇B drift of trapped particles across magnetic surfaces is an origin both of collisionless particle losses as well as enhanced neoclassical transport in the long-mean-free-path regime. Therefore, it is of big interest to compare results for the Γ parameters and for the effective ripple ϵ_{eff}. Figure 5 shows computational results for $\epsilon_{\mathrm{eff}}^{3/2}$ obtained for the first as well as the second QI configurations, for W7-X, and for the $l=3$ magnetic field with $n_p=9$. All results are computed using the technique of Ref. 8.

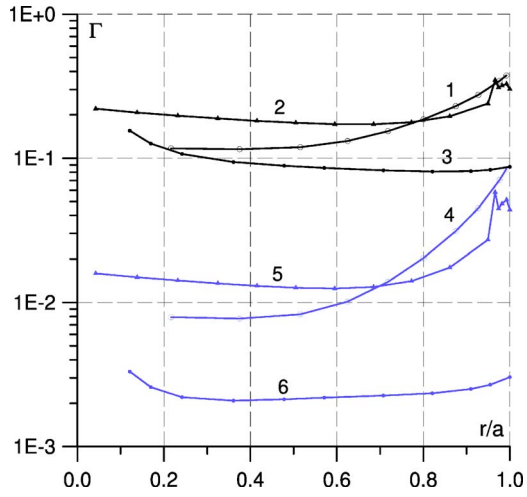

FIG. 4. Factors Γ_w and Γ_v for the magnetic configurations with minimum values of these factors: 1: Γ_v for the second QI configuration; 2: Γ_v for W7-X; 3: Γ_v for the QHS configuration; 4: Γ_w for the second QI configuration; 5: Γ_w for W7-X; 6: Γ_w for the QHS configuration.

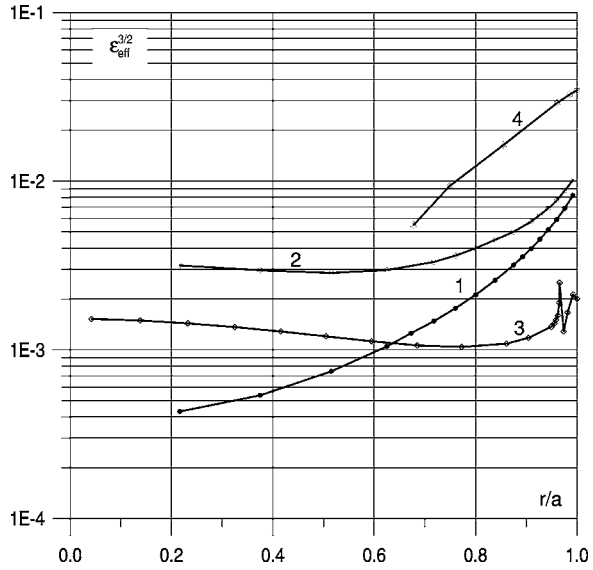

FIG. 5. Factors $\epsilon_{\mathrm{eff}}^{3/2}$ for some of the considered magnetic configurations: 1: first QI configuration; 2: second QI configuration; 3: W7-X; 4: $l=3$ magnetic field with $R_T=10^2$ cm.

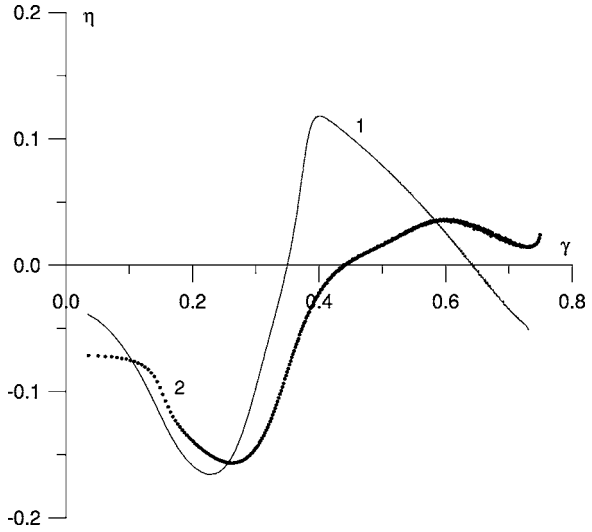

FIG. 6. Characteristic dependencies of η on γ for the magnetic surfaces $r/a=0.718$ of the first QI configuration (curve 1) and of the second QI configuration (curve 2).

As one can clearly see from Fig. 5, the results are again much better than the results for the conventional stellarator. When comparing the results for the first and the second QI configurations, it becomes evident that the final optimization towards poloidal closure of the $J_{\|}$ contours deteriorates the results for $\epsilon_{\mathrm{eff}}^{3/2}$. So, from the viewpoint of $\epsilon_{\mathrm{eff}}^{3/2}$ the first configuration is preferable whereas from the viewpoint of the Γ parameters the second configuration[15] has a clear advantage. This result is in agreement with the results obtained in Ref. 15. Compared to W7-X, the final stage of optimization for the second QI configuration leads to $\epsilon_{\mathrm{eff}}^{3/2}$—values which are at least a factor of 3 larger.

When trying to explain the observed differences one should bear in mind that due to the peculiarities of the Lorentz collision term $\epsilon_{\mathrm{eff}}^{3/2}$ is the square average of v_{an} integrated over the pitch angle with a weight which is specific for the confinement regime. In contrast, the parameters Γ_w and Γ_v are based on the square average of v_{an} only.

Therefore, in a case where v_{an} shows a higher symmetry in the oscillation over the pitch angle, the results for $\epsilon_{\mathrm{eff}}^{3/2}$ turn out to be more favorable than the results for Γ_w and Γ_v. A characteristic example is presented in Fig. 6. Here, the normalized quantity η representing the drift velocity ($v_{\mathrm{an}}=\eta v_{\perp}\rho_L/R_0$) is presented as a function of the pitch γ. One can clearly see that both QI configurations have roughly the same absolute maximum of η and that the strong advantage of the first configuration over the second with respect to $\epsilon_{\mathrm{eff}}^{3/2}$ can only be explained with help of the compensation effect due to the strong oscillation over the pitch angle.

VI. COMPUTATIONS OF THE POLOIDAL MOTION OF TRAPPED PARTICLES

Here, the poloidal motion of trapped particles (55) is studied for three different cases, an $l=2$ conventional stellarator with a magnetic field given in Boozer coordinates in Ref. 17 as well as the two quasi-isodynamic configurations discussed in the previous section. The electric field is assumed to be zero ($\Phi'=0$) because it has only a negligible effect on α-particle motion. In all three cases computations are made for the first 90 local minima of B along a magnetic-field line. The computational results are presented in Figs. 7 and 9, and 10 in a normalized form $d\theta/dt_{\mathrm{norm}}$ as functions of the pitch $\gamma=v_{\|0}/v_{\perp 0}$, where $v_{\|0}$ is $v_{\|}$ at a local minimum of B and $v_{\perp 0}=\sqrt{J_{\perp}B_0}$. The value of $d\theta/dt$ for a deeply trapped particle near the magnetic axis of an $l=2$ stellarator with a large aspect ratio is used for the normalization. With such a normalization, the real value of $d\theta/dt$ is determined as

$$\frac{d\theta}{dt}=\frac{1}{2}\frac{v^2}{\omega_{c0}}\frac{n_p^2}{R^2}\sqrt{\frac{\iota}{n_p}}\left(\frac{d\theta}{dt}\right)_{\mathrm{norm}}. \tag{58}$$

According to Ref. 18, for a stellarator with a large aspect ratio $d\theta/dt$ is determined as

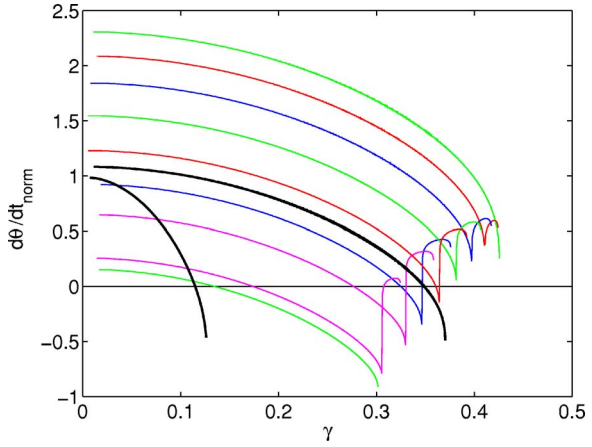

FIG. 7. The normalized $d\theta/dt$ value for the $l=2$ stellarators. Thick curves relate to $n_p=800$ for inner and outer magnetic surfaces. Thin curves relate to different minima of B for $n_p=8$ for the magnetic surface close to the boundary.

$$\frac{d\theta}{dt} = \frac{1}{2} l \frac{v_\perp^2 \epsilon_h}{\omega_c r^2} \left[\frac{2E(\kappa^2)}{K(\kappa^2)} - 1 \right], \tag{59}$$

with $K(\kappa^2)$ and $E(\kappa^2)$ being the complete elliptic integrals of the first and the second kinds, respectively, $(\kappa^2 = v_{\|0}^2/(2\epsilon_h v^2))$. So, for the $l=2$ conventional stellarator with a large aspect ratio $(d\theta/dt)_{\text{norm}}$ is determined as

$$\left(\frac{d\theta}{dt} \right)_{l2,\text{norm}} = \frac{2E(\kappa^2)}{K(\kappa^2)} - 1. \tag{60}$$

Figure 7 gives results for two variants of the $l=2$ stellarator, the first one with an aspect ratio of 10 and the number of field periods $n_p=8$ (thin lines), whereas the second variant has a huge aspect ratio of 1000 and $n_p=800$ (thick lines). This artificial huge number of field periods keeps the length of one field period at the same value. In addition, also the ϵ_h values for both variants are the same.

In the variant with the huge aspect ratio, results in all local minima on a surface show the same behavior: (i) For γ values approaching zero (deeply trapped) the limit of 1 is reached. (ii) The $d\theta/dt$ values equal zero for γ values corresponding to $\kappa^2 \approx 0.83$ (see Ref. 18). This can be found from the relation of κ^2 with γ and ϵ_h using ϵ_h obtained from the distribution of B along the magnetic-field lines. (iii) Except for higher values of γ for which the toroidal effect plays a non-negligible role even in the big aspect ratio case these results are in good agreement with Eq. (60).

The two thick curves in Fig. 7 correspond to a surface with a small mean radius and a smaller value of ϵ_h and to a surface close to the boundary with a larger value of ϵ_h, respectively, thus continuing to larger values of γ.

The thin curves in Fig. 7 show results for the $n_p=8$ variant. These characteristic results belong to a number of local minima of B for a magnetic surface close to the boundary. Now for the lower aspect ratio, the results for different local minima of B are essentially different.

The fact that $d\theta/dt$ becomes zero for certain values of κ^2 is of large significance for stellarators since it leads to very big excursions of the corresponding trapped particles from magnetic surfaces.[18] It can be clearly seen from Fig. 7 that the effect of toroidicity does not remove this feature of $d\theta/dt$ becoming zero for a big fraction of local minima of B.

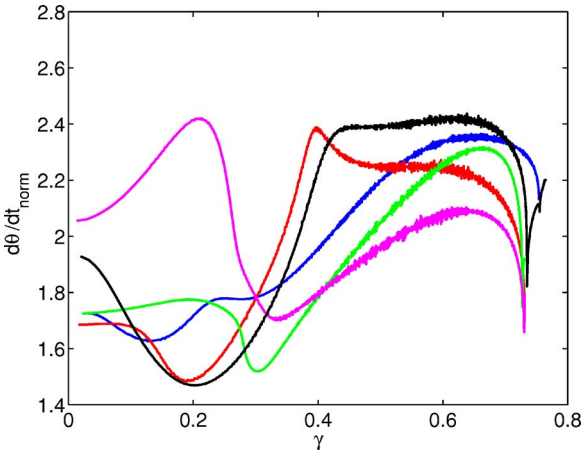

FIG. 9. The normalized $d\theta/dt$ value for the first QI configuration for the magnetic surface $r/a=0.718$.

Using Eqs. (16) and (55), angles between the $J_\|$ contours and the magnetic surface cross section are also assessed as

$$\gamma_{J\|} = \arctan \frac{v_{\text{an}}}{r d\theta/dt}, \quad \gamma_c = \frac{2}{\pi} \gamma_{J\|}, \tag{61}$$

with r being the mean radius of the magnetic surface. Figure 8 presents γ_c which corresponds to the results in Fig. 7 for $n_p=8$. It follows from Fig. 8 that for a rather big fraction of trapped particles $J_\|$ contours are perpendicular to the magnetic surface ($\gamma_c=1$ for $d\theta/dt=0$).

Characteristic results for the first and the second QI configurations obtained for magnetic surfaces at $r/a=0.718$ are presented in Figs. 9 and 10, respectively. The curves represent five characteristic local minima of B out of 90 considered minima. Now, in contrast to the conventional stellarator, the values for $(d\theta/dt)_{\text{norm}}$ stay within the interval of $(1.5, 2.4)$ for both configurations. This is true for all minima in both configurations, so $(d\theta/dt)_{\text{norm}}$ never becomes zero and extremely large excursions of trapped particles do not occur. In addition, the angles between $J_\|$ contours and the magnetic surface cross section are small, $|\gamma_c| \leqslant 0.22$ and

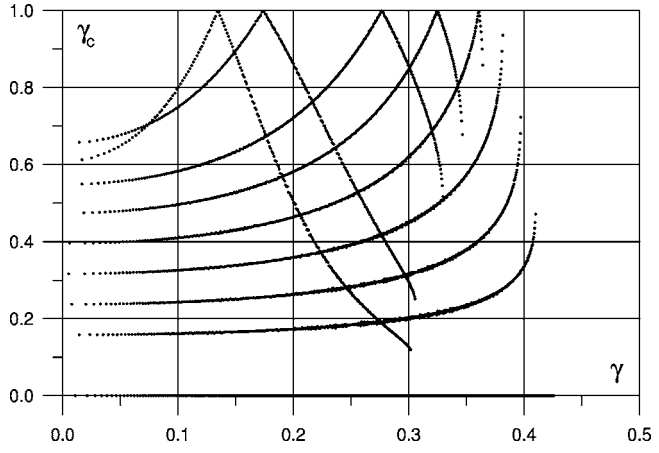

FIG. 8. Parameter γ_c as function of pitch angle for $n_p=8$ and $l=2$ stellarator for the same minima of B as in Fig. 7.

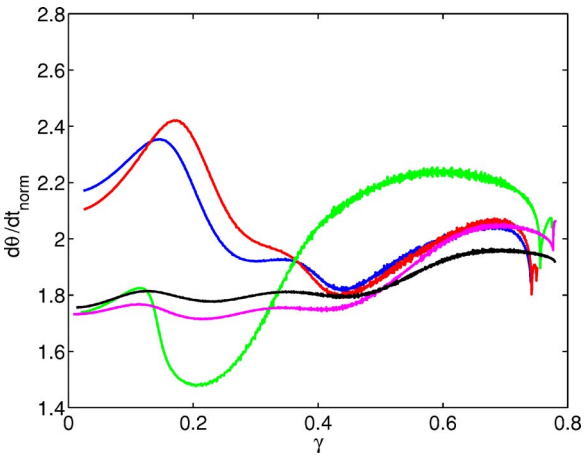

FIG. 10. The same as in Fig. 9 for the second QI configuration.

$|\gamma_c| \leqslant 0.17$ for the first and the second QI configurations, respectively, again reflecting the chosen optimization.

VII. CONCLUSION

The present paper aims at the improvement of targets for stellarator optimization. The main optimization target proposed here is the mean-square average over the pitch angle and over the magnetic surface of the bounce-averaged ∇B drift velocity across magnetic surfaces, $\hat{v}_{\mathrm{an}}$ [(29) and (31)], which is cast into the dimensionless factor Γ_v (28). For a specific configuration, this factor is only a function of the minor radius. It takes into account contributions arising from all kinds of trapped particles which can be trapped within one magnetic-field ripple as well as within several magnetic-field ripples. Another useful target is Γ_w [(21), (23), and (30)] which corresponds to an integral effect of the square of the ∇B drift. Minimization of Γ_v and Γ_w corresponds to the optimization of the trapped particle collisionless confinement being of big importance for α-particle confinement.

Both parameters are calculated using a field line tracing code and the features of the proposed approach are close to the calculation of the effective ripple in Ref. 8. On the other hand, there is an important difference between the Γ factors and the effective ripple resulting from the following fact. In the derivation of the effective ripple, which is the result of a solution of the drift kinetic equation in the $1/\nu$ regime, an important role belongs to collisions represented through the Lorentz collision operator which essentially depends on the particle distribution over pitch angles. Thus, the effective ripple is an interesting measure for transport in a low collisional regime, e.g., relevant for electrons. In contrast to this, the Γ factors do not account for any collisional effects and are therefore well suited for the evaluation of the collisionless particle drift of trapped particles, e.g., fast α particles. This difference can manifest itself in a different functional behavior of the effective ripple and the Γ factors when varying the magnetic field of optimized configurations.

Computations carried out within this work demonstrate this phenomenon. In particular, it can be seen in computations for the optimized quasi-isodynamical configuration of Ref. 15. The Γ_w and Γ_v factors for this configuration are smaller than those for its previous optimization step, whereas $\epsilon_{\mathrm{eff}}^{3/2}$ turns out to be larger compared to the previous optimization step. So, in principle, a simultaneous account for both approaches might be of interest for optimization.

Since field line tracing is used for the computation of the proposed target functions the computation time and the computer resources necessary for their computation turn out to be typically the same as for the NEO code[8] being a fast code which now is effectively used in stellarator optimization problems (e.g., Ref. 2) to analyze the $1/\nu$ transport. So, the new technique is of the same efficiency as the technique used within NEO. It can be applied to any stellarator magnetic field in regions where regular or island magnetic surfaces exist. Calculations can be performed in real-space coordinates or in magnetic coordinates. If the magnetic field is originally available in real-space coordinates calculations can be performed without a field transformation to magnetic coordinates.

A numerical analysis of velocities of the radial drift (16) as well as the poloidal drift (55) allows for a quick assessment of $J_\parallel$ contours in the vicinity of a given magnetic surface. Of course, this has to be done for a variety of positions of local minima of B along a field line and for various pitch angles of trapped particles. This can help to define an interval of the poloidal velocities of trapped particles or a maximum value for the angle between the $J_\parallel$ contours and the magnetic surface cross section. Such quantities, in principle, could also be part of extended optimization strategies. Again, one sees an interesting feature in both QI configurations, namely, the poloidal drift velocity never approaches zero (as it does in a conventional stellarator) but stays within a limited band thus representing the quality of the optimization with respect to the poloidal motion or with respect to closed contours of the second adiabatic invariant.

ACKNOWLEDGMENTS

The authors would like to thank M. I. Mikhailov (RRC "Kurchatov Institute") for the given sets of Boozer data of the quasi-isodynamical stellarator configurations.

This work has been carried out within the Association EURATOM-ÖAW and with funding from the Austrian Science Fund (FWF) under Contract No. P16797-N08.

[1] G. Grieger, W. Lotz, P. Merkel, J. Nührenberg, J. Sapper, E. Strumberger, H. Wobig, the W7-X Team, R. Burhenn, V. Erckmann, U. Gasparino, L. Giannone, H. J. Hartfuss, R. Jaenicke, G. Kühner, H. Ringler, A. Weller, F. Wagner, and the W7-AS Team, Phys. Fluids B **4**, 2081 (1992).
[2] A. Reiman, L. Ku, D. Monticello, S. Hirshman, S. Hudson, C. Kessel, E. Lazarus, D. Mikkelsen, M. Zarnstorff, L. A. Berry, A. Boozer, A. Brooks, W. A. Cooper, M. Drevlak, E. Fredrickson, G. Fu, R. Goldston, R. Hatcher, M. Isaev, C. Jun, S. Knowlton, J. Lewandowski, Z. Lin, J. F. Lyon, P. Merkel, M. Mikhailov, W. Miner, H. Mynick, G. Neilson, B. E. Nelson, C. Nührenberg, N. Pomphrey, M. Redi, W. Reiersen, P. Rutherford, R. Sanchez, J. Schmidt, D. Spong, D. Strickler, A. Subbotin, P. Valanju, and R. White, Phys. Plasmas **8**, 2083 (2001).
[3] R. H. Fowler, J. A. Rome, and J. F. Lyon, Phys. Fluids **28**, 338 (1985).
[4] W. Lotz, P. Merkel, J. Nührenberg, and E. Strumberger, Plasma Phys. Controlled Fusion **34**, 1037 (1992).
[5] L. P. Ku and the ARIES-CS Team, *20th IEEE/NPSS Symposium on Fusion Engineering, San Diego, CA, 14–17 October 2003* (IEEE, New York, 2003), p. 312.
[6] M. Yu. Isaev, M. I. Mikhailov, D. A. Monticello, H. E. Mynick, A. A. Subbotin, L. P. Ku, and A. H. Reiman, Phys. Plasmas **6**, 3174 (1999).
[7] V. V. Nemov, Phys. Plasmas **6**, 122 (1999).
[8] V. V. Nemov, S. V. Kasilov, W. Kernbichler, and M. F. Heyn, Phys. Plasmas **6**, 4622 (1999).
[9] V. V. Nemov, Nucl. Fusion **28**, 1727 (1988).
[10] A. H. Boozer, Phys. Fluids **24**, 1999 (1981).
[11] V. V. Nemov, S. V. Kasilov, W. Kernbichler, and M. F. Heyn, in *28th EPS Conference on Controlled Fusion and Plasma Physics, Funchal, Portugal, 18–22 June 2001*, edited by C. Silva, C. Varandas, and D. Campbell (European Physical Society, Mulhouse, 2001), Vol. 25A, p. 1985.
[12] A. I. Morozov and L. S. Solov'ev, in *Reviews of Plasma Physics*, edited by M. A. Leontovich (Consultants Bureau, New York, 1966), Vol. 2, p. 201 [see also in *Voprosy Teorii Plazmy* (Atomizdat, Moscow, 1963), Vol. 2, p. 177 (in Russian)].
[13] C. Nührenberg, Phys. Plasmas **3**, 2401 (1996).
[14] J. Nührenberg and R. Zille, Phys. Lett. A **129**, 113 (1988).
[15] A. A. Subbotin, W. A. Cooper, M. Yu. Isaev, M. I. Mikhailov, J. Nührenberg, M. F. Heyn, V. N. Kalyuzhnyj, S. V. Kasilov, W. Kernbichler, V. V. Nemov, M. A. Samitov, V. D. Shafranov, and R. Zille, in *29th EPS Conference on Plasma Physics and Controlled Fusion, Montreux, Switzerland, 17–21 June 2002*, edited by R. Behn and C. Varandas (European Physical

Society, Mulhouse, 2002), Vol. 26B, p. 5086.
[16] V. V. Nemov, S. V. Kasilov, W. Kernbichler, M. F. Heyn, and J. Talmadge, in *27th EPS Conference on Controlled Fusion and Plasma Physics, Budapest, Hungary, 12–16 June 2000*, edited by K. Szegö, T. N. Todd, and S. Zoletnik (European Physical Society, Mulhouse, 2000), Vol. 24B, p. 676.
[17] A. H. Boozer and G. Kuo-Petravic, Phys. Fluids **24**, 851 (1981).
[18] A. A. Galeev and R. Z. Sagdeev, in *Reviews of Plasma Physics*, edited by M. A. Leontovich (Consultants Bureau, New York, 1979), Vol. 7, p. 257 [see also in *Voprosy Teorii Plazmy* (Atomizdat, Moscow, 1973), Vol. 7, p. 205 (in Russian)].